

Chromospheric modelling of the $H\alpha$ and Na I D lines in five M dwarfs of low to high activity level

C.I. Short¹ and J.G. Doyle²

¹ Department of Physics & Astronomy, University of Georgia, Athens, GA, 30602-2451, USA (cis@calvin.physast.uga.edu)

² Armagh Observatory, College Hill, Armagh BT61 9DG, Northern Ireland (jgd@star.arm.ac.uk)

Received 23 October 1997 / Accepted 25 May 1998

Abstract. We have obtained simultaneous high resolution $H\alpha$ and Na I D spectra of five dwarf M stars that span a wide range in chromospheric activity level. The observed Na I D lines exhibit behavior that is qualitatively similar to that of more well established diagnostics such as the Ca II HK lines: as the activity level, as indicated by the $H\alpha$ line, increases, the absorption core brightens and then develops an emission reversal. We compare the observed profiles with computed non-LTE profiles from a grid of chromospheric/transition region models. We find that the $H\alpha$ and Na I D lines tend to be in general agreement as indicators of approximate chromospheric activity level. However, the $H\alpha$ line systematically indicates a value for the mass loading at the onset of the Transition Region and the location of T_{\min} that is 0.4 dex lower in column mass density than that indicated by Na I D . Therefore, the profile of both lines cannot be simultaneously well fit for all but one of our stars. We also find, in agreement with the pioneering study of Andretta et al. (1997), that for dMe stars the shape of the Na I D emission cores is a much more sensitive indicator of chromospheric thickness (or, equivalently, chromospheric steepness) than is $H\alpha$, and, therefore, provides a powerful diagnostic complement to $H\alpha$. Finally, we investigate the dependence of the predicted line profiles on the values of the stellar parameters and conclude that the inferred chromospheric pressure is sensitive to the choice of T_{eff} and $\log g$, especially among dMe stars. Specifically, among dMe stars, a model in which the value of T_{eff} is too small or too large by approximately 200 K, or in which the value of $\log g$ is too large or too small by 0.5 dex, will give rise to closest fit values of the column mass density at the location of the Transition Region and T_{\min} that are too small or too large, respectively, by approximately 0.3 dex. As a result, discrepancies between the stellar parameters of our photospheric model and those of the program objects allow us to extract only upper or lower limits for the values of the column mass density at critical points in the chromospheric structure

Key words: stars: late-type – stars: activity – stars: chromospheres – line: formation

1. Introduction

Resonance lines of neutral and singly ionized metals play an important role in the semi-empirical modelling of stellar spectra. Because they are strong and heavily dampened they may be used as probes of the plasma condition over a wide range of depths in the atmosphere from the outer most layers where the line core forms to the continuum forming region where the far wings form. In general, the use of the cores of these lines as plasma diagnostics is complicated by non-LTE effects that necessitate the solution of the coupled radiative transfer and statistical equilibrium equations. One of the ways in which a non-LTE solution may be especially complicated is the dependence of the equilibrium level populations on the non-local radiation field and, hence, on the detailed distribution of radiative opacity throughout the stellar atmosphere. This latter complication is especially problematic in M stars due to the massive over-blanketing of the radiation field by spectral lines from the far UV through to the yellow and red spectral regions.

The study of the outer atmospheric layers of cool stars is especially interesting because these layers exhibit chromospheric and transition region (TR) heating that is not yet fully understood. One way in which we can make progress is to more accurately measure the atmospheric conditions by developing new spectral diagnostics of the outer atmosphere and including them in multi-line model fitting. The value of this approach has been recently underscored by the discovery of an apparent discrepancy between newly developed diagnostics such as the CO $\Delta\nu = 1$ band and traditional diagnostics such as the Ca II HK lines (Ayres 1990).

Andretta et al. (1997, ADB henceforth) investigated the non-LTE behavior of the Na I D lines in a grid of chromospheric/TR models that corresponds to an early dM star and spans a wide range of chromospheric activity levels. They found that the predicted line core responds to increasing chromospheric pressure in a way that is qualitatively similar to that of the well established diagnostics Ca II HK and Mg II hk . As the pressure increases from that of a quiescent, basal chromosphere to that of an active chromosphere, the absorption core first brightens, and then develops a central emission reversal. For those models in which the chromospheric temperature rise is shallower, the line core of the most active models exhibits a double re-

Send offprint requests to: C.I. Short, Department of Physics & Astronomy, University of Georgia, Athens, GA, 30602-2451, USA

Table 1. Program objects

Object	Alternate Name	Activity Level	V	$V - R$
Gl 212	HD233153	dM	9.75	0.94
Gl 382		dM	9.26	0.99
Gl 388	AD Leo	dMe	9.32	1.09
Gl 494	DT Vir	dMe	9.76	0.95
Gl 900		dM(e)	9.52	0.84

versal with a central absorption. As a result, ADB concluded that the Na I D line in early M dwarfs should be a powerful observational discriminator of chromospheric structure. ADB also investigated the effect of including photospheric line blanketing opacity in the calculation of the non-LTE H I and Na I D spectra. They found that the inclusion of background line opacity is especially important for the correct prediction of the line wing flux due to the suppression of the adjacent continuum.

We have obtained high resolution, moderate $S : N$ spectra of a sample of five early dM stars that span a range in chromospheric activity from quiescent to very active. We have re-computed the non-LTE H I and Na I spectra with a treatment of the background line opacity that is more complete than that of ADB (Short & Doyle 1997) and have performed a multi-line fit of a model chromosphere/TR structure to the observed H α and Na I D line core for each of the program stars. In Sect. 2 we describe the observations and data reductions; in Sect. 3 we describe the modelling; in Sect. 4 we present the results of the multi-line fit and compare them to the results of previous studies, and in Sect. 5 we present our conclusions.

2. Observations and reductions

A sample of five early M dwarfs, shown in Table 1, was selected from the combined photometric lists of Leggett (1992) and Stauffer & Hartmann (1986). The selection criteria were: $V < 12$, $0.9 < V - R < 1.3$, $-10^\circ < \delta < +70^\circ$, and $0^h < RA < 12^h$. The $V - R$ criterion limits the MK spectral type to the range of K8 to M4. This constraint was placed on the sample because the extensive line blanketed chromospheric modelling of Short & Doyle (1997, henceforth SD) is limited to models with T_{eff} equal to 3700K, which corresponds to a spectral type of M0 or M1 (Lang 1992, Mihalas & Binney 1981). The sample was chosen to cover a range of chromospheric activity level from low (Gl 212, Gl 382), through intermediate (Gl 900) to high activity level (Gl 388 (AD Leo), Gl 494).

Table 2 contains a journal of the observations. Echellograms centered at $\lambda 6300$ were taken with the Utrecht Echelle Spectrograph (UES) of the William Herchel Telescope (WHT) at the Observatorio Roque de los Muchachos in La Palma on the night of December 23/24, 1996 (JDN=2450441). We used a 79 l mm^{-1} grating that gives $R = 54000$, and a TEK 1024×1024 CCD detector. The H α line falls near the centre of the detector in order 34 and the Na I D doublet falls near the centre in order 38. Multiple exposures with a maximum exposure time of

Table 2. Journal of Observations

Object	Tel	HJD(mid) 2450441+	UT(start)	Exp (s)
Gl 900	WHT	0.34961	20:18:40	700
Gl 900	WHT	0.39108	21:09:13	1800
Gl 900	WHT	0.41612	21:45:17	1800
Gl 212	WHT	0.47609	23:03:32	1800
Gl 212	WHT	0.50119	23:39:41	1800
Gl 212	WHT	0.51896	00:12:46	900
Gl 382	WHT	0.62822	02:46:09	1800
Gl 382	WHT	0.65105	03:19:01	1800
Gl 382	WHT	0.73447	05:19:08	1800
Gl 388	WHT	0.68479	04:06:42	1800
Gl 388	WHT	0.70744	04:39:18	1800
Gl 494	WHT	0.75979	05:59:58	1800
Gl 494	WHT	0.78066	06:32:31	1500
		2448494+		

Table 3. Signal-to-noise values in yellow and red, and W_λ and $FWHM$ (emission) of H α in \AA

Object	Total	Co-added $S : N$	H α	W_λ	$FWHM$
	exp (s)	Na I D	H α	W_λ	$FWHM$
Gl 212	4500	210	280	-0.40	
Gl 382	5400	170	250	-0.38	
Gl 388	3600	190	280	3.44	1.35
Gl 494	3300	140	210	1.38	1.49
Gl 900	4300	260	320	-1.90	

1800 seconds were taken of most objects and were co-added to increase $S : N$. The total $S : N$ values are shown in Table 3.

All reductions were performed with the NOAO Image Reduction and Analysis Facility (IRAF). The stellar frames were corrected by subtraction of the mean of twelve bias frames taken throughout the night, and division by a mean of 32 bias subtracted W lamp flat field frames that were corrected for scattered light (see below) and normalized to a signal level of approximately unity. Cosmic rays were removed from the bias and flat field frames during the calculation of the average frame by σ clipping. Stellar exposure were bracketed by exposures of a Th-Ar arc lamp for wavelength calibration.

Both the mean flat field frame and the stellar frames were found to have significant levels of undispersed background light visible between the echelle orders as a result of internal scattering in the spectrograph. The mean background level varies from exposure to exposure, but was typically 50 to 100 analogue-to-digital conversion units (ADUs) in the stellar frames. A $2D$ function was fit to the background light with a sixth order cubic spline perpendicular to the dispersion and a twelfth order cubic spline parallel to the dispersion. These high order fits were required to approximately fit structure of high spatial frequency in the background scattered light. The fitting was performed interactively and the fits to each row and column were visually inspected to insure that there were no spurious peaks in

the fitting function. The 79 l mm^{-1} grating was used precisely because its wider order separation allows a closer fitting of the background light. Typical RMS deviations from the fit were six ADUs for the fit perpendicular to the dispersion and two ADUs for the fit parallel to the dispersion.

The spectra were extracted using variance weighted extraction (Horne 1986) with a model point spread function (PSF) fit to the strongest stellar exposure of the night. Cosmic rays were removed from the stellar exposures during extraction by σ clipping.

Bright Na I D sky lines were visible in the stellar frames in the inter-order region between order 38 (the Na I D order) and order 37, but, surprisingly, *not* in the region between orders 38 and 39. Therefore, we also extracted a variance weighted sky spectrum from the region between orders 37 and 38. These sky spectra were scaled to compensate for the different aperture sizes used in the stellar and sky extractions and then subtracted from the stellar spectra. Because the star was centered in the slit, the lack of detectable sky lines in the region between orders 38 and 39 is difficult to understand. However, in the context of this work, the important consideration is to be able to extract the profile of the sky lines, which then may be scaled, and subtracted from the stellar spectrum, which we were able to do.

Rectification is complicated by the complete overblanketing of M star spectra in the yellow and red. We obtained a rectification function by fitting a third order Legendre polynomial to the highest peaks of the pseudo-continuum. However, we have probably overestimated the continuum level. We calibrated the wavelength scale of the entire echellogram in each stellar frame by fitting a $2D$ dispersion function to the positions of ≈ 100 lines in the mean of the Th-Ar exposures accompanying the stellar exposure. The RMS deviation is 0.05 \AA .

3. Modelling

ADB have presented a grid of 72 chromospheric and transition region (TR) models in which the photospheric base was computed with PHOENIX (Allard & Hauschildt 1995) and is representative of a dM0 star ($T_{\text{eff}} = 3700 \text{ K}$, $\log g = 4.7$, $[\frac{A}{H}] = 0.0$). The grid explores a wide range in chromospheric pressure from low to high, which corresponds to the range in observed chromospheric activity level from low (dM stars) to high (dMe stars). The grid also explores two values of the chromospheric thickness (or, equivalently, the mean chromospheric temperature gradient), two different functional forms of the chromospheric temperature variation with column mass density, and two different values of the TR thickness. The models of their Series 1A and 2A (chromospheric $\frac{dT}{d \log m} = \text{constant}$) are shown in Fig. 1. ADB computed non-LTE H α and Na I D profiles for this grid. Their calculations included line blanketing opacity, computed with PHOENIX, due to $\approx 70 \times 10^6$ spectral lines of atoms, diatomic molecules, and H_2O . However, this line blanketing opacity was only computed for the photospheric temperature structure below T_{min} . The line opacity was assumed *ad hoc* to approach zero within a decade of logarithmic column mass density above T_{min} .

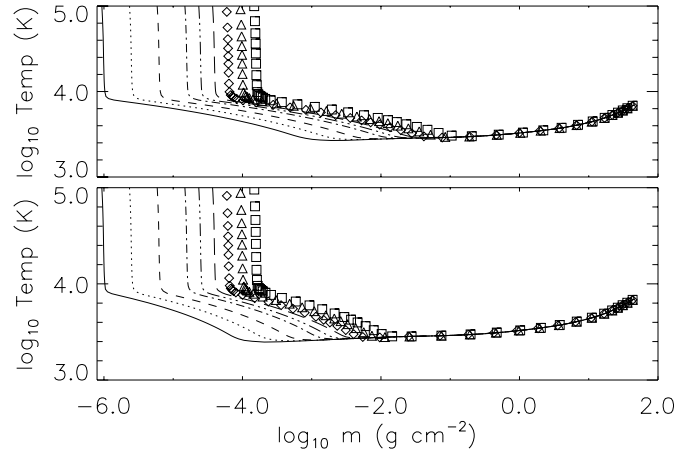


Fig. 1. Temperature structure of models. Upper panel: 1A series, lower panel: 2A series. Solid line: $\log m_{\text{TR}} = -6.0$, dotted line: $\log m_{\text{TR}} = -5.6$, dashed line: $\log m_{\text{TR}} = -5.2$, dot-dashed line: $\log m_{\text{TR}} = -4.8$, dot-dot-dot-dashed line: $\log m_{\text{TR}} = -4.6$, long dashed line: $\log m_{\text{TR}} = -4.4$, diamonds: $\log m_{\text{TR}} = -4.2$, triangles: $\log m_{\text{TR}} = -4.0$, squares: $\log m_{\text{TR}} = -3.8$

SD recomputed the PHOENIX line opacity spectrum for a small sub-grid of six models within Series 1A and 2A of the grid of ADB. This opacity calculation differed from that of ADB in that the line opacity was calculated throughout the entire atmospheric model using the chromospheric and TR temperature structure as input to the opacity calculation. As a result, the background line blanketing opacity is consistent with the chromospheric/TR temperature structure of the outer atmosphere. SD found that in a chromospheric model the line blanketing opacity initially *increases* with declining column mass density in the low chromosphere above T_{min} , in sharp contrast to the assumption of monotonically decreasing chromospheric line opacity made by ADB. The complete, self-consistent line blanketing opacity has now been computed for the eighteen models presented here using the procedure described in SD.

SD used the MULTI non-LTE radiative transfer code (Carlsson 1986) to recompute the non-LTE H I spectrum with their complete line blanketing opacity included in the calculation and compared the resulting line profiles with those resulting from the adoption of the line blanketing of ADB. They found that for the most active (dMe) models, the complete treatment of line blanketing opacity is necessary to correctly model the Ly α and H α lines. Figs. 5 through 13 show the computed H α profiles, and Table 4 gives the W_λ values of the predicted H α lines and the $FWHM$ values for those models that have H α in emission. A comparison of the computed W_λ values with those for the sub-grid treated by SD shows discrepancies, with the W_λ values given here being variously smaller or larger than the previous value by as much as 32%. The reason for the discrepancy is an improved treatment of the optical depth grid spacing in the calculation of the statistical equilibrium and radiative transfer problem for Hydrogen. Negative W_λ values indicate net absorption.

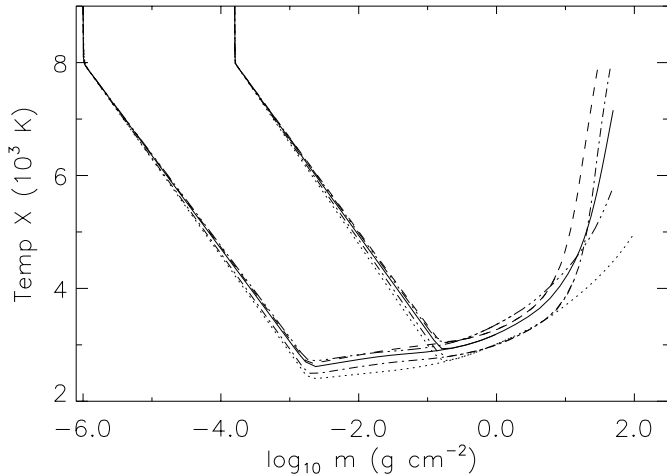


Fig. 2. Grid of models with low ($\log m_{\text{TR}} = -6.0$) and high ($\log m_{\text{TR}} = -3.8$) chromospheric pressure that explores a range of photospheric stellar parameters. Solid line: $T_{\text{eff}} = 3700$ K, $\log g = 4.5$ (model closest to that used for entire grid), dotted line: $T_{\text{eff}} = 3400$ K, $\log g = 4.5$, dashed line: $T_{\text{eff}} = 3900$ K, $\log g = 4.5$, dot-dashed line: $T_{\text{eff}} = 3700$ K, $\log g = 4.0$, dot-dot-dot-dashed line: $T_{\text{eff}} = 3700$ K, $\log g = 5.0$.

Table 4. Computed H α line: W_{λ} and $FWHM$ (emission) in \AA

Model $\log m_{\text{TR}}$	Series 1A		Series 2A	
	W_{λ}	$FWHM$	W_{λ}	$FWHM$
-6.0	-0.07		-0.05	
-5.6	-0.24		-0.18	
-5.2	-0.56		-0.49	
-4.8	-0.59		-0.43	
-4.6	-0.10		0.13	
-4.4	1.09	1.42	1.31	1.24
-4.2	3.03	1.45	3.10	1.27
-4.0	5.50	1.48	5.52	1.30
-3.8	8.47	1.52	8.67	1.34

We have also used MULTI to recompute the non-LTE Na I spectrum using the model atom that was described by ADB, but with our complete line blanketing included in the background opacity. Figs. 6 through 14 show the computed Na I D_2 profiles. ADB and SD contain extensive detailed discussions of the effect of different line blanketing treatments on the calculated non-LTE H I and Na I spectra. Here we will confine our discussion to the comparison with the observed spectra.

3.1. Dependence on stellar parameters

The reported values of T_{eff} found in the literature for our program stars span the range from 3270 K (Gl 388) to 3870 K (Gl 494). The value of $\log g$ for these stars has not been measured and previous investigators normally adopt values around 5.0 on the basis of spectral type when modelling the atmosphere. The actual value is not likely to differ from this by more than ≈ 0.5 dex if these stars have a luminosity class of type V. Our pho-

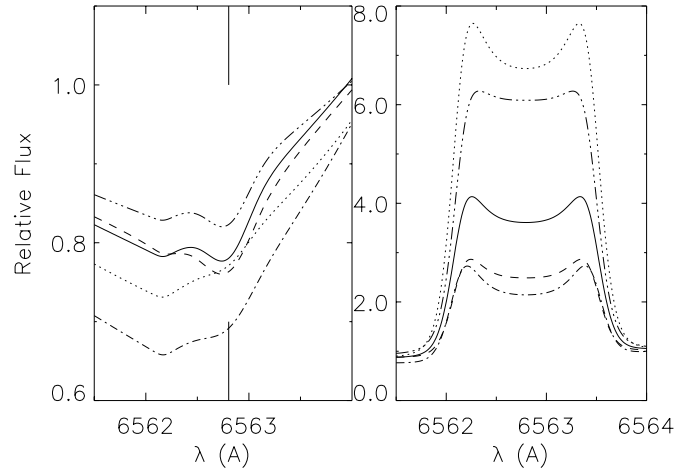


Fig. 3. Synthetic H α profile for models of fixed chromospheric/TR structure and varying stellar parameter. Left panel: models with chromosphere/TR structure of low pressure ($\log m_{\text{TR}} = -6.0$), right panel: models with chromosphere/TR structure of high pressure ($\log m_{\text{TR}} = -3.8$). Vertical lines in left panel indicate the position of H α . Solid line: $T_{\text{eff}} = 3700$ K, $\log g = 4.5$ (model closest to that used for entire grid), dotted line: $T_{\text{eff}} = 3400$ K, $\log g = 4.5$, dashed line: $T_{\text{eff}} = 3900$ K, $\log g = 4.5$, dot-dashed line: $T_{\text{eff}} = 3700$ K, $\log g = 4.0$, dot-dot-dot-dashed line: $T_{\text{eff}} = 3700$ K, $\log g = 5.0$.

tospheric base model has T_{eff} and $\log g$ values of 3700 K and 4.7, respectively. Therefore, we investigate the sensitivity of the predicted line profiles to variation in the stellar parameters by computing the H I and Na I spectra for models with $\log g$ equal to 4.5 and T_{eff} equal to 3400 and 3900 K, and for models with T_{eff} equal to 3700 K and $\log g$ equal to 4.0 and 5.0.

The grid of models used in the perturbation analysis is shown in Fig. 2. For each set of stellar parameters we have attached the chromospheric/TR structure of Series 1A with the lowest and highest value of the chromospheric pressure. We then compute line profiles for the grid. In this grid of models we have held the value of m_{Tmin} fixed. Therefore, because the temperature structure below T_{min} is different for models with different values of the stellar parameters, the value of T_{min} is necessarily different in each of these models. The total range in T_{min} throughout the grid is about 400 K. It is not possible to hold both m_{Tmin} and T_{min} fixed when attaching chromospheric structures to radiative equilibrium photospheric models with different temperature structures. We have chosen to construct a perturbation analysis grid in which m_{Tmin} rather than T_{min} is held constant, and some of the variation in the predicted H I and Na I spectra will be due to the variation in T_{min} as well as the variation of T_{eff} and $\log g$.

The results of this perturbation analysis can be seen in Figs. 3 and 4. The blanketed line profile have been approximately normalized in relative flux by a single point division by the calculated value of the continuum flux at the wavelength of H α . With the expanded relative flux scale of the left panel in Fig. 3 we can see the difference in the shape of the pseudo-continuum due to the different line opacity distributions for models of different parameters.

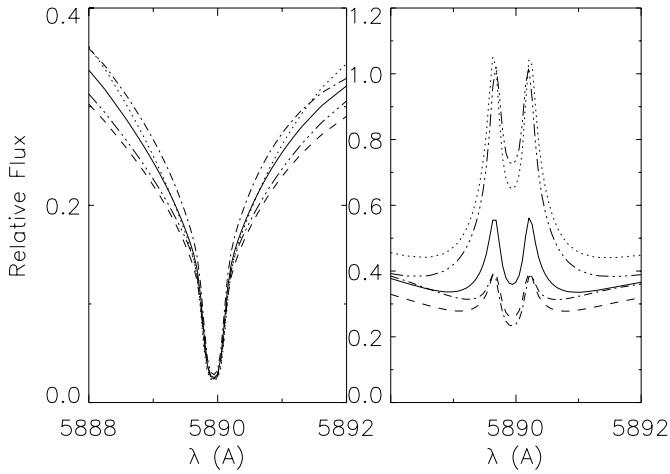


Fig. 4. Synthetic Na I D profile for models of fixed chromospheric/TR structure and varying stellar parameter. See Fig. 3 caption.

3.1.1. Low pressure chromosphere

$H\alpha$ For the low pressure chromospheric models of the left panel of Fig. 3, $H\alpha$ shows a significant T_{eff} dependence: the absorption line is almost undetectable in the $T_{\text{eff}} = 3400$ K model and is broader and stronger by about 0.05 in relative flux in $T_{\text{eff}} = 3900$ K model. We note that the computed $H\alpha$ line is blended with the background line blanketing opacity. Therefore, some of the T_{eff} dependence may be due to differences in the background line opacity at the wavelength of $H\alpha$, rather than to changes inherent in the $H\alpha$ transition itself. The relative line strength is almost identical in the models with $\log g$ equal to 4.5 and 5.0, but is noticeable weaker in the model with $\log g$ equal to 4.0. However, comparing the difference between the profiles for the models of varying T_{eff} and $\log g$ of low chromospheric pressure in Fig. 3 to the difference between models of varying chromospheric pressure in Fig. 5, we can see that in the regime of low chromospheric pressure the change in the line profile due to variation in the stellar parameters is significantly less than the change due to a step in chromospheric pressure in the chromospheric/TR grid.

$Na I D$ The left panel of Fig. 4 shows that the model with T_{eff} equal to 3400 K and that with $\log g$ equal to 4.0 have inner wings that are about 0.025 brighter, and the model with T_{eff} equal to 3900 K, and that with $\log g$ equal to 5.0, have inner wings that are about 0.025 darker, than the fiducial model. At the same time, all models have almost identical central core profiles. Therefore, there is a slight dependency of the inner wing-to-core contrast on the stellar parameters. From comparison with the low pressure synthetic line profiles in Fig. 6 (those with $-6.0 < \log m < -4.6$), we note that the dependency of the inner wing-to-core contrast on stellar parameters is of the same size as the dependency on the location of $\log m_{\text{TR}}$.

3.1.2. High chromospheric pressure

$H\alpha$ The right panel of Fig. 3 shows that varying stellar parameters have a large effect on the predicted strength of $H\alpha$ when it is in emission. Changing T_{eff} from 3700 K to 3400 K, or increasing $\log g$ from 4.5 to 5.0 approximately doubles the flux at line center, $F_{\nu}(\Delta\lambda = 0)$, and the equivalent width, W_{λ} . This change is equivalent to increasing the value of $\log m_{\text{TR}}$ in the chromospheric grid by 0.3 dex in the high pressure regime where $H\alpha$ is in emission. The T_{eff} dependency, in which emission strength relative to the local continuum varies inversely with T_{eff} may be partially understood as a contrast effect in which an emission line that forms in a fixed chromospheric/TR structure is being seen against a photospheric background of varying brightness temperature. However, a proper understanding of the dependency would require a detailed analysis of radiative transfer quantities such as intensity contribution functions and monochromatic source function throughout the line profile and adjacent continuum, as has been done in the case of chromospheric H I line formation by Short & Doyle (1997). The results of the perturbation study in the regime of high chromospheric pressure place severe limitations on the accuracy of chromospheric modelling of dMe stars with the $H\alpha$ line.

$Na I D$ The right panel of Fig. 4 shows that, as in the case of $H\alpha$, modest variation in T_{eff} and $\log g$ changes $F_{\nu}(\Delta\lambda = 0)$ and W_{λ} by approximately a factor of two or more. As with $H\alpha$, a reduction of T_{eff} or an enhancement of $\log g$ causes a dramatic increase in the emission line contrast with the local continuum. The general observation made above for H I holds for Na I; a proper understanding of the difference in line profile in different models requires an in depth radiative transfer analysis such as that provided for the chromospheric Na I spectrum by ADB.

Application to this study The results of the perturbation study in the regime of high chromospheric pressure place severe limitations on the accuracy of chromospheric modelling of dMe stars with the $H\alpha$ and Na I D line. Unless the fundamental stellar parameters are known accurately, the closest fit chromospheric/TR structure is not well constrained. A proper analysis should employ a grid that spans a range of T_{eff} and $\log g$ values as well as a range of chromospheric/TR parameters. However, due to the enormous computational effort required to compute complete line blanketing opacity for a unified chromospheric/TR structure, we hold T_{eff} and $\log g$ fixed at 3700 K and 4.7 throughout the chromospheric modelling of individual stars and use the results of the perturbation analysis as a guide to the limitations on the accuracy of the modelling. Most of the stars in our sample do not have reported abundance measurements. Therefore, for the same reason of computational expediency, we have held $[\frac{A}{H}]$ fixed at 0.0.

If we attempt to fit either $H\alpha$ or the Na I D core of an active (dMe) star that has a value of T_{eff} that is *higher* than that of our model (3700 K), then the model will predict emission cores that are too bright with respect to the adjacent continuum (too

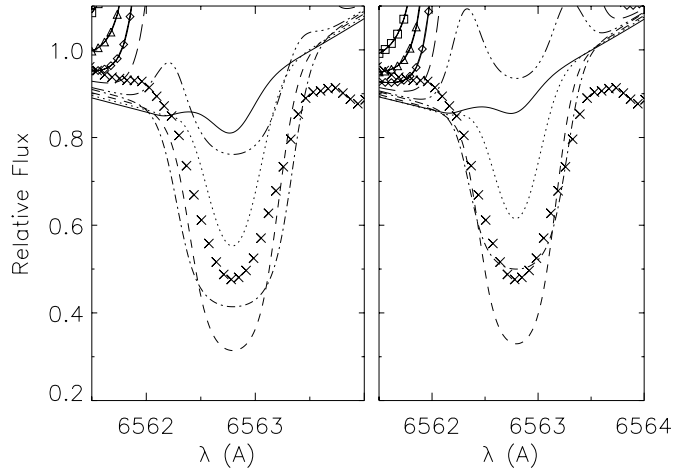


Fig. 5. Gl 212, $H\alpha$. Left panel: models of 1A series, right panel: models of 2A series. Crosses: observed spectrum. Models in order of increasing chromospheric pressure as measured by $\log m_{\text{TR}}$: solid line: $\log m_{\text{TR}} = -6.0$, dotted line: $\log m_{\text{TR}} = -5.6$, dashed line: $\log m_{\text{TR}} = -5.2$, dot-dashed line $\log m_{\text{TR}} = -4.8$, dot-dot-dot-dashed line: $\log m_{\text{TR}} = -4.6$, long dashed line: $\log m_{\text{TR}} = -4.4$, diamond line: $\log m_{\text{TR}} = -4.2$, triangle line: $\log m_{\text{TR}} = -4.0$, square line: $\log m_{\text{TR}} = -3.8$

contrast) for a given value of $\log m_{\text{TR}}$. Noting the dependence of the predicted $H\alpha$ profile on $\log m_{\text{TR}}$ shown in Fig. 9, we see that the inaccuracy in T_{eff} will mimic the effect of a larger value of $\log m_{\text{TR}}$, which will be compensated for by reducing the value of $\log m_{\text{TR}}$ to achieve a close fit. As a result, the inferred value of $\log m_{\text{TR}}$ will be too small, and will be a lower limit to the actual value. Similarly, the closest fit value of $\log m_{\text{TR}}$ will be an upper limit in the case where we fit a star with a value of T_{eff} lower than that of our model.

If we attempt to fit the absorption core of the Na I D line in the spectrum of a low activity (dM) star that has a value of T_{eff} that is *higher* than 3700 K, then the model will predict a line profile in which the contrast between the inner wing and Doppler core is too large. By noting the dependence of the predicted line profiles in Fig. 6, we see that the inaccuracy in T_{eff} will mimicking the effect of lower $\log m_{\text{TR}}$. This will be compensated for by raising the value of $\log m_{\text{TR}}$ in the model to achieve a good fit. Therefore, the value of $\log m_{\text{TR}}$ derived from the fit will be too large, and will, thus, be an upper limit.

4. Results

4.1. Individual stars

4.1.1. Gl 212

Notes Alonso (1996) used the Infrared Flux Method and ATLAS9 (Kurucz 1990) models to measure T_{eff} and found 3832 K. He adopted values of $\log g$ and $[\frac{A}{H}]$ equal to 5.0 and 0.0, respectively. Spectral types of dM1, dM2.5, and dM2 have been reported by Poveda et al. (1994), Eggen (1996), and Rutten et al. (1989), respectively. Measured emission fluxes in well known chromospheric lines such as Ca II HK and Mg II hk can be

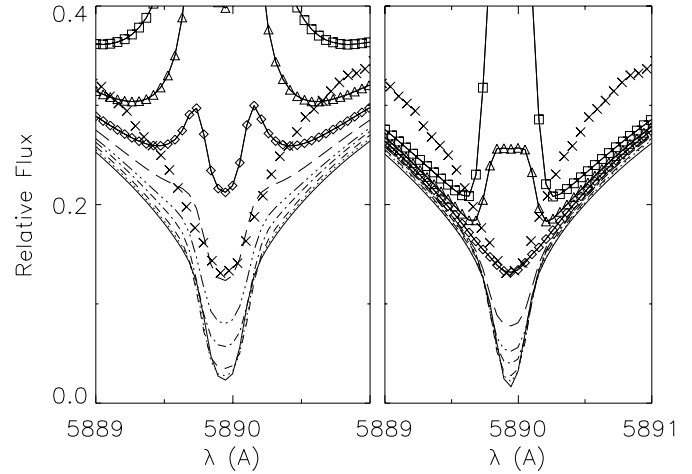


Fig. 6. Gl 212, Na I D_2 . See Fig. 5.

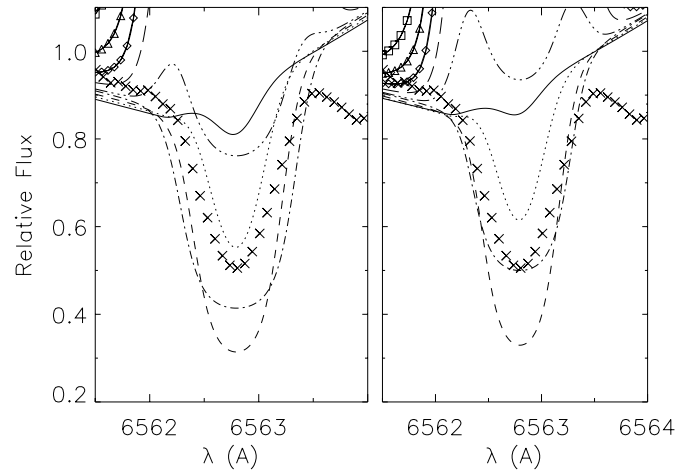


Fig. 7. Gl 382, $H\alpha$. See Fig. 5.

found, variously, in Panagi & Mathioudakis (1993), Rutten et al. (1989), and Giampapa et al. (1989). In their large catalogue of measured $W_\lambda(H\alpha)$ values, Stauffer & Hartmann (1986) give -0.31\AA (the negative sign indicates that $H\alpha$ is in absorption).

$H\alpha$ We measure W_λ to be -0.40 , which is stronger by 25% than the value of Stauffer & Hartmann (1986). From Table 4 we see that the predicted value of W_λ of $H\alpha$ in *absorption* first grows, then declines with increasing $\log m_{\text{TR}}$. Therefore, the closest fit to both of these measured values of W_λ could be provided by a model with a value of $\log m_{\text{TR}}$ between -5.6 and -5.2 or between -4.8 and -4.6 . The comparison of the observed and computed $H\alpha$ line profiles is shown in Fig. 5. We note that while the region to the blue of $H\alpha$ is generally well fit by the synthetic spectrum, the region to the red is very poorly fit. The line list that was used to calculate the synthetic spectrum was constructed with the goal of accurately reproducing broad and intermediate band photometric diagnostics (Kurucz 1990), rather than for the detailed fitting of high resolution spectra. Therefore, the line list is pervaded by inaccuracies in the oscillator strengths and transition wavelengths that cause local

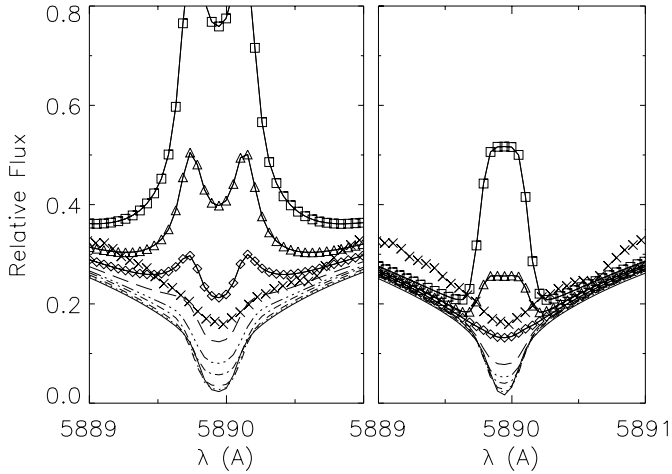


Fig. 8. Gl 382, Na I D_2 . See Fig. 5.

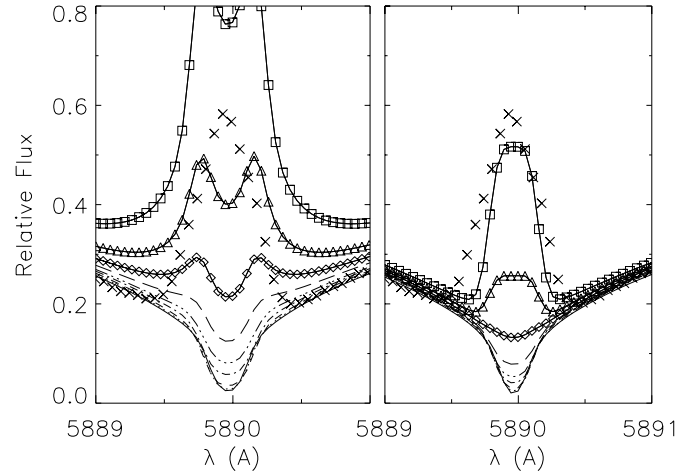


Fig. 10. Gl 388, Na I D_2 . See Fig. 5.

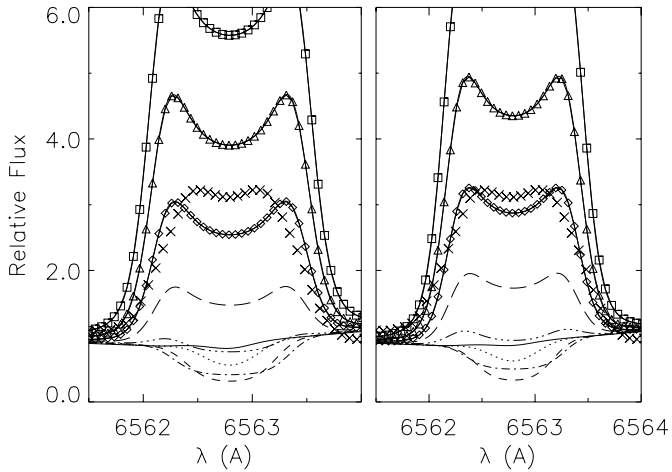


Fig. 9. Gl 388, H α . See Fig. 5.

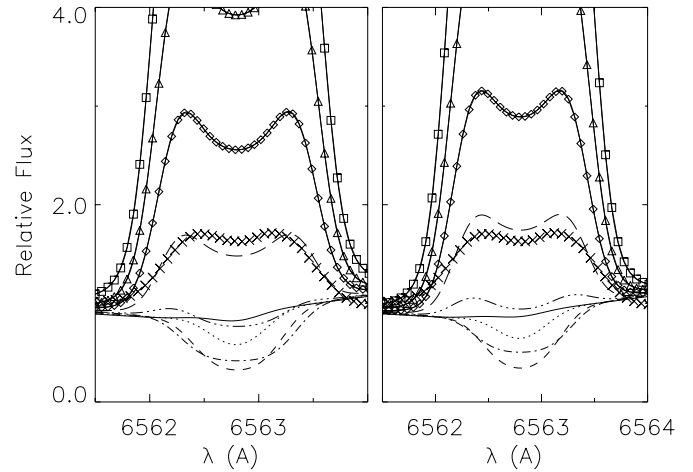


Fig. 11. Gl 494, H α . See Fig. 5.

discrepancies in high resolution fit. In Fig. 5 we see that for a given value of $\log m_{\text{TR}}$, Series 1A models produce line profiles that are deeper and wider than those of Series 2A. A close fit to the shape of the observed line profile is provided by a model of either series with $\log m_{\text{TR}}$ between -5.6 and -5.2 or a model of Series 2A with $\log m_{\text{TR}} \approx -4.8$, in agreement with the closest fit indicated by the value of W_λ . The measured T_{eff} of Gl 212 is hotter than that of our model by ≈ 130 K Alonso (1996). On the basis of the perturbation analysis shown in Fig. 3, we expect the line profile to be minimally affected by variation in T_{eff} in the low pressure, absorption line regime.

Na I D From Fig. 6 we see that models of Series 1A give rise to line profiles in which the core is wider than those of Series 2A. Also, within each Series, the three models of lowest chromospheric pressure all give rise to line profiles that are almost identical. Therefore, we cannot expect the Na I D line to be an effective discriminator of chromospheric structure among inactive dM stars. The core of the observed line profile is in absorption, which corresponds to the behavior of the models of low chromospheric pressure. However, the synthetic spectra are

too depressed in the inner wings and core by as much as ≈ 0.05 in relative flux, despite having been rectified to the observed pseudo-continuum. From the perturbation analysis of Fig. 4, we note that for a model with a value of T_{eff} that is too low we expect the model to predict *too much* flux in the inner wings. Therefore, the discrepancy cannot be explained by the inaccurate value of T_{eff} in the model. Nevertheless, the *shape* of the inner wings is approximately fit by models with $\log m_{\text{TR}}$ between -6.0 and -5.2 . However, the contrast between the inner wings and core are fit most closely by a model with $\log m_{\text{TR}}$ between -4.8 and -4.6 . A model with too low a value of T_{eff} will predict too large an inner wing-to-core contrast, which mimics the effect of lower $\log m_{\text{TR}}$. Therefore, the value of $\log m_{\text{TR}}$ derived from a fit to the contrast is an upper limit. In any case, models of Series 1A fit the width of the observed line core better than those of Series 2A.

Simultaneous fit Both lines can be fit approximately with a model of Series 1A with a value of $\log m_{\text{TR}}$ between -5.2 and -5.6 . Series 2A models are ruled out by the width of the Na I D line core, and models of Series 1A with $\log m_{\text{TR}}$ between

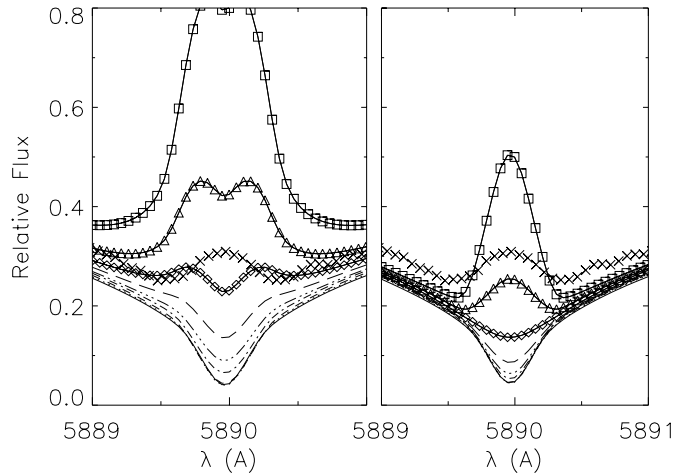


Fig. 12. Gl 494, Na I D_2 . See Fig. 5.

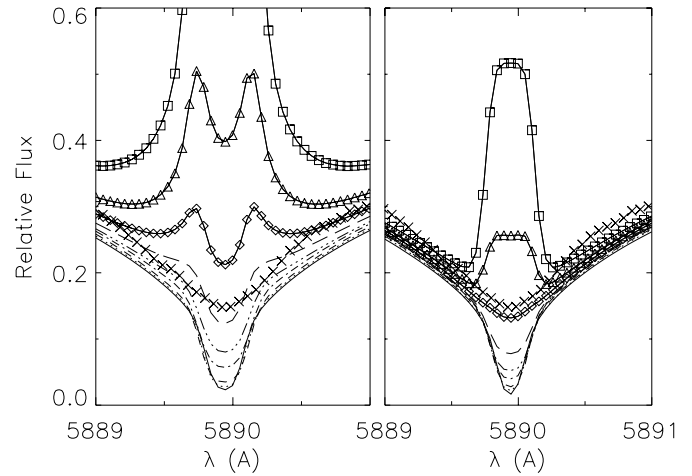


Fig. 14. Gl 900, Na I D_2 . See Fig. 5.

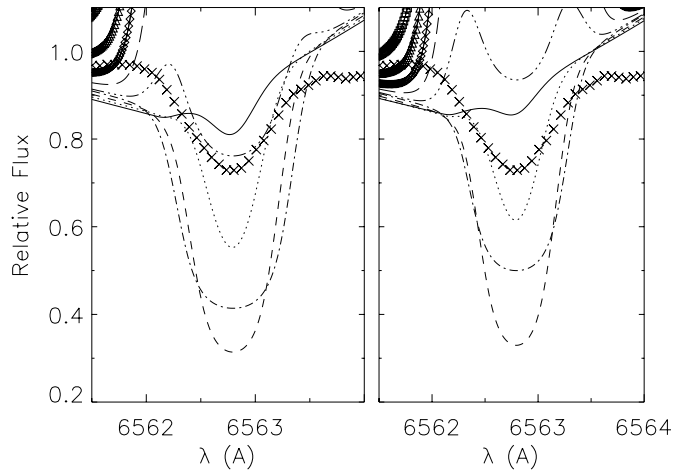


Fig. 13. Gl 900, H α . See Fig. 5.

−4.8 and −4.6 are ruled out by the narrowness of the observed H α core.

4.1.2. Gl 382

Notes Mathioudakis & Doyle (1991) give $T_{\text{eff}} = 3415$ K and a spectral type of dM2. Eggen (1996) also reports a spectral type of dM2. Panagi & Mathioudakis (1993), Giampapa et al. (1989), and Mathioudakis & Doyle (1991) report integrated flux values for various chromospheric emission lines. Stauffer & Hartmann (1986) and Mathioudakis & Doyle (1991) give $W_{\lambda}(\text{H}\alpha)$ equal to -0.37 and -0.23\AA , respectively.

H α We measure W_{λ} to be -0.38\AA , in close agreement with the value of W_{λ} of -0.37 measured by Stauffer & Hartmann (1986), but higher than the value of -0.23 measured by Mathioudakis & Doyle (1991). From Table 4 we see that, like Gl 212, all three of these measured values of W_{λ} indicate either $\log m_{\text{TR}}$ between -5.6 and -5.2 , or between -4.8 and -4.6 . From Fig. 7, we see that the observed line profile is similar to that of Gl 212, but slightly weaker. Again, the closest fit is provided by a model of

either series with $\log m_{\text{TR}}$ between -5.6 and -5.2 . However, in this case, models of both series with $\log m_{\text{TR}}$ greater than -5.2 are ruled out by the narrowness of the observed line core. The measured temperature of Gl 382 is almost 300 K lower than that of our model (Mathioudakis & Doyle 1991). From the perturbation analysis of Fig. 3, we expect a model that is too hot to overpredict the strength of H α in the low chromospheric pressure regime. Therefore, the values of $\log m_{\text{TR}}$ derived here are lower limits.

Na I D From Fig. 8 we see that, for the low pressure models, the model that is fit most closely by the shape of the inner wings and that which is fit most closely by the contrast of the inner wing to the core are even more discrepant than was the case for Gl 212. However, a *higher pressure* model of Series 2A with $\log m_{\text{TR}}$ between -4.0 and -4.2 provides a close fit throughout the entire inner line profile. We see from Fig. 4 that, among models of lower chromospheric pressure, a model with too large a value of T_{eff} will underpredict the contrast of the inner wing to core, mimicking the effect of higher $\log m_{\text{TR}}$. Therefore, the value of $\log m_{\text{TR}}$ is a lower limit. However, this T_{eff} dependency is slight and is not able to fully explain how the observed line profile, which has almost no detectable absorption core, could arise from a low pressure model such as that required to fit H α .

Simultaneous fit The closest fit value of $\log m_{\text{TR}}$ found from the Na I D line is over an order of magnitude greater in column mass density than that required to fit H α . Indeed, the value of $\log m_{\text{TR}}$ required to fit Na I D gives rise to an H α profile that is strongly in *emission*, whereas the observed H α profile is clearly in *absorption*. Furthermore, the dependency of both line profiles on the value of the stellar parameters cannot account for the entire discrepancy.

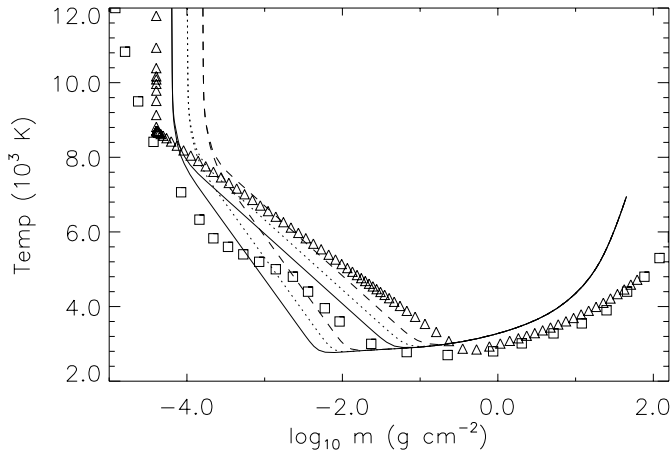


Fig. 15. Temperature structure of models corresponding to GJ 388. The Series 2A models are the ones with lower $m_{T\min}$ values and steeper chromospheric T distributions. Solid line: $\log m_{\text{TR}} = -4.2$, dotted line: $\log m_{\text{TR}} = -4.0$, dashed line: $\log m_{\text{TR}} = -3.8$. Squares: best fit model of Mauas & Falchi (MF model) (1994), triangles: quiescent model of Hawley & Fisher (HF model) (1992).

4.1.3. GJ 388

Notes GJ 388 (AD Leo) is a well known flare star (Pettersen 1991). Giampapa et al. (1989) and Malyuto et al. (1997) report spectral types of dM4Ve and dM4.5Ve, respectively. Fleming et al. (1995) report solar metallicity, while Naftilan et al. (1992) found $[\frac{A}{H}] = -0.4$ from spectrum synthesis. Caillault & Patterson (1990) found $T_{\text{eff}} = 3267$. Panagi & Mathioudakis (1993), Rutten et al. (1989), Giampapa et al. (1989), Doyle et al. (1990), Pettersen & Hawley (1989), Herbst & Miller (1989), and Elgaroy et al. (1990) give measured flux values in a variety of chromospheric emission lines including, variously, H α , Ly α , Ca II HK and Mg II hk . Doyle (1996), Mathioudakis et al. (1995), and Byrne & Doyle (1989) report fluxes in a variety of FUV and EUV lines that form in the TR. Stauffer & Hartmann (1986) and Pettersen & Hawley (1989) give $W_{\lambda}(\text{H}\alpha)$ values of 3.43 \AA and 4.0 \AA , respectively. The positive value indicates net emission. Stauffer & Hartmann (1986) also give $FWHM(\text{H}\alpha) = 1.18\text{\AA}$. Young et al. (1989) find a range in the value of *excess* $W_{\lambda}(\text{H}\alpha)$ of 2.57 to 3.91 \AA . MacMillan & Herbst (1991) found the value of $W_{\lambda}(\text{H}\alpha)$ to range from 2.7 \AA to 3.53 \AA with $\sigma = 0.311$. The minimum value of $W_{\lambda}(\text{H}\alpha)$ is interpreted as corresponding to a “quiet” photosphere, analogous to the quiet Sun, and the variation in $W_{\lambda}(\text{H}\alpha)$ is interpreted to be due to a combination of spots and flares. Dempsey et al. (1993) in their data compilation give $v \sin i = 8 \text{ km s}^{-1}$. Marcy & Chen (1992), on the basis of four lines in high resolution spectra derive $v \sin i = 5.6 \pm 0.5 \text{ km s}^{-1}$.

The most extensive atmospheric modelling effort to date is that of Mauas & Falchi (1996), who performed two component, 2D chromospheric/TR modelling in the 1.5D approximation of the *flaring* atmosphere. They fit simultaneously the H γ , H δ , Ca I 4227, and Ca II K lines. This followed an earlier modelling effort by Mauas & Falchi (1994) in which they constructed 1D chromospheric/TR models to fit simultaneously the H α , H β ,

H γ , H δ , Ca I 4227, Ca II K , Ca II 8498, Mg I b , Na I D , and Na I 8183/95 lines, and the optical continuum. Fig. 15 shows the temperature structure of the quiescent model.

H α We measure W_{λ} to be 3.4 \AA , which falls between the values of 2.7 and 4.0 found by MacMillan & Herbst (1991) and Pettersen & Hawley (1989), respectively. From Table 4 we see that this range in W_{λ} can be accommodated by a very narrow range of models in the grid as result of the large sensitivity of $W_{\lambda}(\text{H}\alpha)$ to changes in $\log m_{\text{TR}}$. Our observed value and that of MacMillan & Herbst (1991) may be fit by a model of either series with $\log m_{\text{TR}}$ between -4.2 and -4.0 . We measure the $FWHM$ of the emission core to be 1.35 \AA , which is somewhat greater than the value of 1.18 \AA found by Stauffer & Hartmann (1986). The latter value is narrower than that predicted by any model in either series. However, our value may be approximately fit by a model of Series 2A with $\log m_{\text{TR}}$ equal to -3.8 .

The theoretical profiles have been rotationally broadened with a value of $v \sin i$ equal to 5.6 km s^{-1} (Marcy & Chen 1992). In Fig. 9 we see that the closest fit model provided by either series has $\log m_{\text{TR}}$ approximately equal to -4.2 . The emission profiles of Series 2A are narrower and have less pronounced central self-absorption reversals than those of Series 1A and provide a better fit to the observed profile. The measured value of T_{eff} for GJ 388 is over 400 K less than that of our model (Caillault & Patterson 1990). From Fig. 3 we see that high pressure chromospheric models that are too hot will predict emission lines that are too weak. Therefore the values of $\log m_{\text{TR}}$ that are found by our H α fitting are upper limits.

Na I D In Fig. 10, for models that have emission cores, the Na I D core shows a much greater discrimination between the two model series than does H α , with Series 1A yielding profiles that have a clear central double reversal, and Series 2A yielding profiles with a single reversal. As a result, the D_2 emission core very clearly distinguishes the highest pressure model from Series 2A as the closest fit. In particular, a Series 2A model with $\log m_{\text{TR}}$ equal to -3.8 provides an approximate fit. As in the case of H α , the high value of T_{eff} in the model yields line profiles that are too weak for a given value of $\log m_{\text{TR}}$. Therefore, the value of $\log m_{\text{TR}}$ derived here is an upper limit.

Simultaneous fit Both lines have emission cores and, therefore, require high pressure chromospheres. However, the value of $\log m_{\text{TR}}$ required by the H α line is 0.4 dex lower in column mass density than that required to fit Na I D_2 . The discrepancy may in part be due to the high sensitivity of the emission strength to small changes in $\log m_{\text{TR}}$, especially in the case of H α , and in part due to the inaccuracy of the value of T_{eff} used in the model, which limits the fit to a derivation of an upper limit only on the value of $\log m_{\text{TR}}$. The greater sensitivity of Na I D to chromospheric thickness and steepness allows us to identify Series 2A as the closest fit.

Comparison with previous models Mauas & Falchi (1994) derived a semi-empirical atmospheric model of the quiescent state of AD Leo (henceforth the MF model) by fitting several spectral features observed by Pettersen & Hawley (1989) with synthetic spectra calculated with the PANDORA (Avrett & Loeser 1992) model atmosphere code: the over all continuum, the profiles of the first four members of the Balmer series, Na I D , Mg I b , and Ca II K and $\lambda 8499$ lines, and the total fluxes of the Ly α and Mg II h and k lines. They include the effect of line blanketing in their calculation by incorporating the line lists of Kurucz (1990), but it is unclear whether the line blanketing is calculated self-consistently for the entire model with the chromospheric/TR temperature rise, or if it is included for the photosphere only. Their model is shown in Fig. 15 along with models from both of our series with $\log m_{\text{TR}}$ between -3.8 and -4.2 , which spans the range in $\log m_{\text{TR}}$ that was fit separately by either of our diagnostics.

The chromospheric $T(\log m)$ structure of their model is more general than ours in that it deviates from a straight line. However, the mean slope is close to that of our Series 1A models. The location of T_{min} in the MF model is close to that of our highest pressure model. The value of $\log m_{\text{TR}}$ falls within the range spanned by our closest fit models, but the TR temperature rise of the MF model is much more gradual than that of ours.

One possible reason for the discrepancies between the MF model and ours is the difference in the spectral resolution of the data being fit. We fit fully resolved profiles of emission cores, whereas the data of Pettersen & Hawley (1989) have a resolution, $\Delta\lambda$, of 3.5\AA , which is not sufficient to resolve the detailed shape of the line profile. For example, the central absorption reversal of the $H\alpha$ emission core in dMe stars is a diagnostic of the TR slope (Houdebine et al. 1995), and our Series 2A model fits the reversal approximately. By contrast, the observed $H\alpha$ spectrum used by Mauas & Falchi does not resolve the central reversal. Similarly, the slope, $T(\log m)$ of the chromospheric temperature rise is distinguished in our fitting by the presence or absence of a central absorption reversal in the Na I D core, whereas the emission cores are not resolved at all in the data of Pettersen & Hawley (1989).

Another reason for discrepancies in the chromospheric/TR structure between our model and the MF model is the difference in the photospheric structure of the two models. The photospheric temperature structure of the MF model is flatter than ours, and we have already seen from the perturbation analysis presented in Figs. 3 and 4 that the calculated profiles of chromospheric features depend sensitively on the structure of the underlying photosphere. Because Mauas & Falchi derived the structure of the *photosphere*, as well as the chromosphere, semi-empirically, we cannot assign the usual stellar parameters to their model for the sake of comparison with our photospheric model. However, from Fig. 15, we also see that the MF model corresponds to a lower value of T_{eff} than ours, and is, therefore, in better agreement with the measured T_{eff} value of Gl 388. From the perturbation analysis given above, we expect that a model with a lower photospheric T_{eff} would give rise to a close

fit chromospheric structure with lower values of the column mass density, as does the MF model.

Fig. 15 also shows the model of AD Leo of Hawley & Fisher (1992) (henceforth the HF model). The photospheric base is provided by a model of Mould (1976) that corresponds to T_{eff} equal to 3500 K, $\log g$ equal to 4.75, and $[\frac{A}{H}]$ equal to 0.0. The temperature structure of the chromosphere and upper photosphere of this model was computed theoretically by adopting a model for the overlying corona and assuming that coronal X-ray illumination is the source of excess heating in the outer atmosphere during quiescence. The energy equilibrium structure is computed by balancing the coronal X-ray heating against the radiative losses in the H I spectrum and the Mg II hk and Ca II HK lines. The procedure was iterated with re-integration of the hydrostatic equilibrium equation.

The value of $\log m_{\text{TR}}$ in the HF model is 0.2 dex less than that of the lowest pressure model that approximately fits either of our diagnostics. Also, the location of T_{min} is almost 0.3 dex deeper than our well fitting model with the deepest T_{min} . Furthermore, the slope, $T(\log m)$, of the chromospheric temperature rise is similar to that of our Series 1A models, which are clearly ruled out by the lack of a central absorption reversal in the observed Na I D lines. However, the HF model is purely theoretical and has not been fit to any observed chromospheric diagnostics. Also, as with the MF model, the underlying photosphere has a flatter temperature structure, and, indeed, corresponds to a T_{eff} value that is 200 K lower than that of our model. On the basis of the perturbation analysis shown in Fig. 3, the amount of the radiation loss in the H I spectrum, which is important in determining the structure of the HF model, will be affected by the photospheric structure.

4.1.4. Gl 494

Notes Alonso (1996) finds $T_{\text{eff}} = 3870$ K by the Infrared Flux Method, having adopted values of $\log g$ and $[\frac{A}{H}]$ equal to 5.0 and 0.0, respectively. Rutten et al. (1989) give a spectral type of dM2e and Henry et al. (1994) find a type of dM3V. Panagi & Mathioudakis (1993), Rutten et al. (1989), Doyle et al. (1990), Pettersen & Hawley (1989), Herbst & Miller (1989), and Panagi et al. (1991) give measured flux values in various chromospheric emission lines, including the Na I D lines in the case of the latter. Stauffer & Hartmann (1986) give $W_{\lambda}(H\alpha) = 2.12$ and $FWHM(H\alpha) = 1.20\text{\AA}$, while Panagi et al. (1991) give $FWHM(H\alpha) = 1.37\text{\AA}$ and the ratio of line centre to continuum flux, $\frac{F_{\alpha}}{F_c}$, equal to 2.01. Pettersen & Hawley (1989) give $W_{\lambda}(H\alpha) = 3.3\text{\AA}$ and Young et al. (1989) find the range in *excess* $W_{\lambda}(H\alpha)$ to be 1.80 to 2.54\AA . Panagi et al. (1991) report self-reversals in the cores of the Na I D doublet in WHT spectra. Stauffer & Hartmann (1986) find $v \sin i = 10 \text{ km s}^{-1}$.

$H\alpha$ We measure W_{λ} to be 1.4\AA , which is just below the range of the previous measurements of 2.12, 1.48, and 3.3\AA (Stauffer & Hartmann 1986, Panagi et al. 1991, Pettersen & Hawley 1989). From Table 4, a model with $\log m_{\text{TR}}$ between -4.4 and

–4.2 provides a fit to our measured value and those of Stauffer & Hartmann (1986) and Panagi et al. (1991). We measure the $FWHM$ of the emission core to be 1.49\AA , which is slightly larger than the value of $FWHM = 1.37\text{\AA}$ found by Panagi et al. (1991) and significantly smaller than the value of 2.12\AA found by Stauffer & Hartmann (1986). Our measured value may be fit by a model of Series 1A with $\log m_{\text{TR}}$ between -3.8 and -4.0 , whereas the value of Panagi et al. (1991) and Stauffer & Hartmann (1986) lie outside the range predicted by either series.

The synthetic profiles have been rotationally broadened with a value of $v \sin i$ of 10.0 km s^{-1} (Stauffer & Hartmann 1986). We see from Fig. 11 that, in keeping with the closest fit to the value of W_λ , models with $\log m_{\text{TR}} = -4.4$ of either series provide close fits to the observed profile, although the slightly closer spacing of the emission peaks of the Series 2A model provides a slightly better fit. Because the T_{eff} value of this star is over 150 K hotter than that of the model, we expect, according to Fig. 3, that the model will predict emission lines that are too strong for a given value of $\log m_{\text{TR}}$. Therefore, the value of $\log m_{\text{TR}}$ fit here is a lower limit.

Na I D Unlike the synthetic H α profiles, the synthetic Na I D profiles distinguish very clearly between the two model series. The presence of a central self-absorption reversal in the Series 1A models rules them out as good fits. A model of Series 2A with $\log m_{\text{TR}} \approx -4.0$ provides a close fit to the shape of the line core, although the predicted profile is lower in flux than the observed one by ≈ 0.03 in relative flux throughout the entire inner line profile. This discrepancy may be due to inaccuracy of the rectification of the observed to the computed pseudo-continuum, or due to inaccuracy in the stellar parameters of the photospheric model. However, from Fig. 4, we expect that a model with too low a value of T_{eff} will predict *too much* flux in the inner wings rather than too little. As with H α , the inaccuracy in the model value of T_{eff} leads us to take the value of $\log m_{\text{TR}}$ derived here as a lower limit.

Simultaneous fit The value of $\log m_{\text{TR}}$ that is found from a fit to the H α line is 0.4 dex smaller in column mass density than that found from a fit to the Na I D_2 core. Indeed, the value found from the H α profile corresponds to a model in which the Na I D core is in *absorption*, whereas the observed core is clearly in emission. The discrepancy may in part be due to the inaccuracy of the model T_{eff} value, which makes our derived values of $\log m_{\text{TR}}$ from each line lower limits only.

4.1.5. G1 900

Notes G1 900 is unique in our sample because it is the only "zero H α " (dM(e)) star. There are no measured values of T_{eff} reported in the literature. Byrne & Doyle (1989) report fluxes in a variety of FUV lines that form in the TR and find that they are intermediate between those of quiescent dM and active dMe stars. From high resolution spectroscopy, Robinson & Cram (1989) find that the Ca II core flux is intermediate between that

of dM and dMe stars. They also find that the H α profile has emission wings and an absorption core.

Rutten et al. (1989) give a spectral type of dM1. Panagi & Mathioudakis (1993), Rutten et al. (1989), Giampapa et al. (1989), Herbst & Miller (1989), and Robinson et al. (1990) give measured flux values in a variety of chromospheric emission lines. Stauffer & Hartmann (1986) give $W_\lambda(\text{H}\alpha) = 0.01$. Fleming et al. (1989), from moderate resolution spectroscopy, measure $v \sin i < 10 \text{ km s}^{-1}$.

H α Although G1 900 has been found to be a zero H α star, we detect a distinct absorption line, although it is much weaker than that of G1 212 or G1 382. We measure W_λ to be -0.2\AA , which is smaller than the values of 0.01 and 0.08 found by (Stauffer & Hartmann 1986, Robinson et al. 1990). The latter two values correspond to slight emission, rather than absorption. From Table 4 we see that in Series 2A all three measured values may be fit with a model with $\log m_{\text{TR}}$ between -4.8 and -4.6 . Among Series 1A models, our value corresponds to a model with $\log m_{\text{TR}}$ between -4.8 and -4.6 and those of Stauffer & Hartmann (1986) and Robinson et al. (1990) indicate a model with $\log m_{\text{TR}}$ between -4.6 and -4.4 . In Fig. 13 the depth and width of the observed line profile is approximately fit by a model of Series 1A with $\log m_{\text{TR}}$ equal to -4.6 . However, this model has small but significant emission wings that are not present in the observed line profile. A model with a value between -4.6 and -4.8 , which would be deeper but have weaker or absent emission wings may provide a better fit, in agreement with the results of the W_λ fit. The Series 2A profiles of the same $\log m_{\text{TR}}$ range are slightly narrower and, therefore, provide a slightly worse fit.

Na I D In Fig. 14 we can see that a model of Series 2A with $\log m_{\text{TR}}$ equal to -4.2 provides a very close fit to the shape of the entire inner line profile. None of the models of Series 1A is able to provide even an approximate fit.

Simultaneous fit The Na I D_2 line profile is almost perfectly fit by a model in which the value of $\log m_{\text{TR}}$ is larger by at least 0.4 dex in column mass density than that needed to fit H α . The usual caveats about inaccuracies in the stellar parameters of the model apply, although we cannot provide a quantitative assessment due to the lack of measured values of the parameters in the literature. In the case of G1 900, the ability to simultaneously fit both lines is complicated by another consideration: the "zero-H α " stars of intermediate chromospheric pressure exist in a regime where both H α and the Na I D line cores are making a very rapid transition from being in absorption to being in emission with increasing $\log m_{\text{TR}}$. Therefore, the strength and shape of each line is more sensitive to slight changes in $\log m_{\text{TR}}$ as compared to the low chromospheric pressure regime. As a result, unless the detailed modelling of the line formation and detailed structure of the models is very accurate, we may not expect to be able to fit both lines even approximately with a single model.

5. Conclusions

We have presented the first systematic exploration of the Na I D lines in early M dwarfs of various activity levels. We have confirmed the prediction of ADB that these lines show similar behavior to that of previously known chromospheric diagnostics such as Ca II HK : a brightening of the line core with increased chromospheric pressure that culminates in a central emission reversal in the highest activity models.

For the dMe stars of high chromospheric pressure (Gl 388, Gl 494) and the one dM(e) ("zero $H\alpha$ ") star of intermediate chromospheric pressure, the model that provides the closest fit to the $H\alpha$ line has a value of $\log m_{\text{TR}}$ that is approximately 0.4 dex lower in column mass density than that which provides the closest fit to the Na I D_2 core. The discrepancy is significant in the sense that the model that provides the closest fit to one of these lines cannot even approximately fit the other. However, the discrepancy is small enough that models fit to each line are in the same general regime of chromospheric pressure. The consistency of the discrepancy among the three different stars suggests a systematic effect. For the dMe stars the Na I D_2 line cores are in emission and the determination of the chromospheric thickness (model series) that fits most closely the star is determined entirely by the shape of the core. Whereas the $H\alpha$ line profile is negligibly affected by the chromospheric thickness (or, equivalently, chromospheric steepness), the Na I D emission core is affected significantly, varying from a double peaked profile with a clear central absorption reversal for the thicker Series 1A models to a single peaked profile for the thinner Series 2A models. For this reason, the Na I D line core is a powerful diagnostic complement to the $H\alpha$ line for active M dwarfs.

The two dM stars of low chromospheric pressure (Gl 212, Gl 382) are unique in their ability to be fit. For Gl 212 we are able to fit both lines closely with a model of the same value of $\log m_{\text{TR}}$ and the same chromospheric thickness. By contrast, the closest fit model to the $H\alpha$ line of Gl 382 has a value of m_{TR} that is approximately an order of magnitude lower than that which fits most closely the Na I D core. For the dM stars, in which both lines have cores that are in absorption, neither line distinguishes chromospheric thickness as clearly as the Na I D emission core does for the dMe stars.

An important caveat to the use of either emission line is the sensitivity of the computed emission core contrast to the adopted value of both T_{eff} and $\log g$. Lowering or raising T_{eff} by ≈ 200 K approximately doubles or halves the predicted brightness contrast of the emission core. Lowering or raising $\log g$ by ≈ 0.5 dex has a similar effect. As a result, the value of the chromospheric pressure that is inferred from a closest fit may be incorrect by an amount corresponding to 0.3 dex in the mass loading at the onset of the TR and the location of T_{min} . Given the uncertainties in measured stellar parameters due to the faintness of M dwarfs, and the lack of $\log g$ measurements, this places significant uncertainties on the modelling of emission spectra in active M dwarfs.

Acknowledgements. The main body of this work has been carried out at Armagh Observatory, supported by PPARC grant GR/K04613. We also acknowledge support at Armagh in terms of both software and hardware by the STARLINK Project, funded by the UK PPARC. The WHT is operated on the island of La Palma by the Isaac Newton Group in the Spanish Observatorio del Roque de los Muchachos of the Instituto de Astrofísica de Canarias.

References

- Allard, F., & Hauschildt, P. H., 1995, *ApJ*, 445, 433
 Alonso, A., Arribas, S., & Martinez-Roger, C., *A&AS*, 1996, 117, 227
 Andretta, V., Doyle, J. G., & Byrne, P. B., 1997, *A&A*, 322, 266 (ADB)
 Avrett, E. H. & Loeser, R., 1992, in *The 7th Cambridge Workshop on Cool Stars, Stellar Systems, and the Sun*, eds. M. Giampapa and J. A. Bookbinder
 Ayres, T. R., 1990, in *IAU Symposium 138, Solar Photosphere: Structure, Convection, and Magnetic Fields*, ed. J. O. Stenflo, (Dordrecht: Kluwer), p. 23
 Byrne, P. B. & Doyle, J. G., 1989, *A&A* 208, 159
 Byrne, P. B., Eibe, M. T., & Rolleston, W. R. J., 1996, *A&A*, 311, 651
 Byrne, P. B. & McKay, D., 1990, *A&A* 227, 490
 Caillault, J.-P. & Patterson, J., 1990, *AJ*, 100, 825
 Carlsson, M., 1986, Uppsala Observatory Internal Report no. 33
 Dempsey, R. C., Bopp, B. W., Henry, G. W., & Hall, D. S., 1993, *ApJS*, 86, 293
 Doyle, J. G., 1996, *A&A* 307, 45L
 Doyle, J. G. & Collier Cameron, A., 1990, *MNRAS* 244, 291
 Doyle, J. G., Panagi, P., & Byrne, P. B., 1990, *A&A* 228, 443
 Eggen, O. J., 1996, *AJ*, 111, 466
 Elgaroy, O., Engvold, O., & Carlsson, M., 1990, *A&A* 234, 308
 Fleming, T. A., Gioia, I. M., & Maccacaro, T., *ApJ*, 340, 1011
 Fleming, T. A., Schmitt, J. H. M. M., & Giampapa, M. S., 1995, *ApJ*, 450, 401
 Giampapa, M. S., Cram, L. E., & Wild, W. J., 1989, *ApJ*, 345, 536
 Hawley, S. L. & Fisher, G. H., 1992, *ApJS*, 78, 565
 Hempelmann, A., Schmitt, J. H. M. M., Schultz, M., Ruediger, G., & Stepien, K., 1995, *A&A* 294, 515
 Henry, T. J., Kirkpatrick, J. D., & Simons, D. A., 1994, *AJ*, 108, 1437
 Herbst, W. & Miller, J. R., 1989, *AJ*, 97, 891
 Horne, K., 1986, *PASP*, 98, 609
 Houdebine, E. R. & Doyle, J. G., 1994, *A&A*, 289, 169
 Houdebine, E. R., Doyle, J. G., & Kosciielecki, M., 1995, *A&A*, 294, 773
 Jeffries, R. D., James, J. D., & Bromage, G. E., *MNRAS*, 271, 476
 Kurucz, R. L., 1990, in *Transactions of the IAU, XXB*, ed. M. McNally, (Dordrecht: Kluwer), p. 168
 Lang, K. R., 1992, *Astrophysical Data: Planets and Stars*, (Springer-Verlag: New York)
 Leggett, K. S., 1992, *ApJS*, 82, 351
 MacMillan, J. & Herbst, W., 1991, *AJ* 101, 1788
 Malyuto, V., Oestreich, M. O., & Schmidt-Kaler, T., 1997, *MNRAS*, 286, 500
 Marcy, G. W. & Chen, G. H., 1992, *ApJ* 390, 550
 Mathioudakis, M. & Doyle, J. G., 1991, *A&A* 244, 409
 Mathioudakis, M., Fruscione, A., Drake, J. J., McDonald, K., Bowyer, S., & Malina, R. F., 1995, *A&A* 300, 775
 Mauas, P. J. D. & Falchi, A., 1996, *A&A* 310, 245
 Mauas, P. J. D. & Falchi, A., 1994, *A&A* 281, 129
 Mihalas, D. & Binney, J., 1981, *Galactic Astronomy*, 2nd ed., (W. H. Freeman and Co.)

- Mould, J. R., 1976, A&A 48, 443
- Naftilan, S. A., Sandmann, W. S., & Pettersen, B. R., 1992, PASP, 104, 1045
- Panagi, P. M., Byrne, P. B., & Houdebine, E. R., 1991, A&AS, 90, 437
- Panagi, P. M. & Mathioudakis, M., 1993, A&AS 100, 343
- Pettersen, B. R., 1991, Mem. Soc. Astron. Ital. 62, 217
- Pettersen, B. R. & Hawley, S. L., 1989, A&A 217, 187
- Poveda, A., Herrera, M. A., Allen, C., Cordero, G., & Lavalley, C., 1994, Rev. Mex. Astron. Astrofis., 28, 43
- Robinson, R. D. & Cram, L. E., 1989, Proc. Astron. Soc. Australia, 8, 132
- Robinson, R. D., Cram, L. E., & Giampapa, M. S., 1990, ApJS, 74, 891
- Rutten, R. G. M., Schrijver, C. J., Zwaan, C., Duncan, D. K., & Mewe, R., 1989, A&A, 219, 239
- Schwartz, R. D., Dawkins, D., Findley, D., & Chen, D., PASP, 107, 667
- Short, C. I. & Doyle, J. G., 1997, A&A, 326, 287
- Soderblom, D. R., 1990, AJ 100, 204
- Stauffer, J. R. & Hartmann, L. W., 1986, ApJS, 61, 531
- Stepien, K., 1994, A&A 292, 191
- Ungren, A. R. & Caruso, J. R., 1988, AJ, 96, 719
- Ungren, A. R., Dawson, D. W., & Lu, P. K., 1981, ApJ, 251, 557
- Young, A., Skumanich, A., Harlan, E., 1984, ApJ, 282,
- Young, A., Skumanich, A., MacGregor, K. B., & Temple, S., 1990, ApJ, 349, 608
- Young, A., Skumanich, A., Stauffer, J. R, Bopp, B. W., & Harlan, E., 1989, ApJ, 344, 427